ELSEVIER

Thermochimica Acta 247 (1994) 225–236

thermochimica acta

High-temperature heat capacities and electrical conductivities of UO_2 doped with simulated fission products for 2–10 at% burnup

Yuji Arita, Seiichi Hamada, Tsuneo Matsui *

Department of Nuclear Engineering, Faculty of Engineering, Nagoya University, Furo-cho, Chikusa-ku, Nagoya 464-01, Japan

Received 10 February 1994; accepted 19 May 1994

Abstract

Using samples prepared by the same method as for a previously prepared 10% burnup sample, heat capacities and electrical conductivities of UO_2 doped with simulated fission products equivalent to 2 and 5 at% burnup were measured simultaneously with a direct heating pulse calorimeter over the range 290–1500 K to confirm the presence of an anomalous increase in the heat capacity curve of UO_2 doped with 10% simulated fission products previously found by the present authors. In addition, using a new sample of UO_2 doped with 10% burnup simulated fission products prepared by a different method and, having better homogeneity of the dopants in UO_2 than the previous samples, measurements of heat capacity and electrical conductivity were carried out in order to investigate the effect of different sample characteristics on the heat capacity anomaly. An anomalous increase in the heat capacity curve was seen in each sample, and those of two 10% burnup UO_2 samples were much the same, indicating that the anomalous increase is inherent and does not depend on the sample character. The origin of the heat capacity anomaly was also discussed in comparison with that of UO_2 doped with a single kind of cation reported previously.

Keywords: Burnup; Conductivity; Doping; Fission product; Heat capacity; Uranium oxide

1. Introduction

The mechanical properties and irradiation behaviour of UO_2 have been reported to be modified by doping with a small amount of aliovalent cations such as Ti, Nb

* Corresponding author.

SSDI 0040-6031(94)01911-Y

and La [1]. The heat capacities of UO_2 doped with Gd, La, Sc, Ti, Nb, Eu, Y have been measured in our laboratory from room temperature to 1500 K using a direct heating pulse calorimeter [2–6], and an anomalous increase in the heat capacity curve of each sample of UO_2 doped with trivalent cations such as Gd [2], La [3], Sc [4], Eu [5] and Y [6] was observed from 700 to 1300 K, depending on the kind of dopant and its concentration. The heat capacity of UO_2 doped with Gd was also measured using differential scanning calorimetry and drop calorimetry by Mills et al. [7] and a similar anomalous increase in the heat capacity curve was observed. The heat capacity of UO_2 doped with simulated fission products has recently been measured by two groups [6,8]. Matsui et al. [6] measured the heat capacity of UO_2 doped with simulated fission products (without noble metals), all of which are soluble in UO_2 matrix, equivalent to 10 at% burnup, by means of direct heating pulse calorimetry in the temperature range from 300 to 1500 K and found an anomalous increase in the heat capacity curve above about 600 K, which is similar to the cases of UO_2 doped with a single kind of aliovalent cation [2–6]. Lucuta et al. [8] also measured the heat capacities of UO_2 doped with simulated fission products including noble metals, which precipitate in UO_2 matrix, equivalent to 3 and 8 at% burnup, using differential scanning calorimetry below 900 K and by the drop method at higher temperatures between 700 and 1600 K, and reported slightly higher heat capacities of UO_2 doped with simulated fission products than that of undoped UO_2 over the entire temperature range from 300 to 1700 K.

In the present study, both the heat capacities and the electrical conductivities of UO_2 doped with simulated fission products equivalent to 2 and 5 at% burnup were measured simultaneously by direct heating pulse calorimetry over the range from 290 to 1500 K to confirm the presence of an anomalous increase in the heat capacity curve of UO_2 doped with 10% simulated fission products previously reported by the present authors [6]. In addition, the measurements of heat capacity and electrical conductivity were carried out on a new UO_2 sample doped with 10 at% burnup simulated fission products, for which the size (diameter and length) and preparation method (sintering temperature and holding time) are different from those of the sample doped with the same amount of 10% burnup simulated fission products previously prepared [6], in order to investigate the effect of the difference in the sample characteristics on the heat capacity anomaly. The origin of an anomalous increase in the heat capacity curve is also discussed in comparison with the previous results for UO_2 doped with a single kind of cation.

2. Experimental

2.1. Direct heating pulse calorimeter

The heat capacity and the electrical conductivity were measured simultaneously by direct heating pulse calorimetry, the details of which are given elsewhere [9]. In this calorimeter, the temperature of a sample rod was at first increased up to a desired temperature by an external platinum heater, and after reaching equilibrium

(after a constant desired temperature), electric power was then supplied directly to the sample rod in a short period (usually 1 s) through a regulated d.c. power supply and the temperature rise of the sample (generally 2–5 K) was measured by a Pt/Pt-13%Rh thermocouple. In order to reduce the error in the heat capacity due to heat leak from the sample at high temperature, a double cylindrical thermal shield made of molybdenum, placed outside the sample, was simultaneously heated electrically with a sample rod using batteries so as to obtain the same temperature rise as the sample, i.e. to attain the adiabatic condition. The electric potential drop, the current and the temperature rise of the sample rod were measured to obtain the heat capacity and the electrical conductivity for the same sample simultaneously. The heat capacity measurement has an error of $\pm 2\%$, which was estimated by comparing the heat capacity of undoped UO_2 determined in this study with the previous literature values [6,10].

2.2. Sample preparation and characterization

Two series (A and B) of samples of UO_2 simulating high burnup were prepared. The simulated elements selected as the representative components of the fission products in this study are all soluble major fission products, except the volatile elements and noble metals, as shown in Table 1. In the case of the A series of samples (FP2A (2 at% burnup) and FP5A (5 at% burnup)), five elements (such as Zr, Ce, Pr, Nd and Y) were selected as the representative fission products and the dopant concentrations (in atomic percent) in UO_2 were determined on the basis of the table of the fission yield of stable or long-lived fission products [11], as was selected in the previous studies on the oxygen potential of UO_2 fuel simulating 2–10 at% burnup by Une and Oguma [12] and the heat capacity determined by the present authors [6]. However, it has recently been reported that Sr may be soluble in UO_2 instead of forming separated zirconates and/or uranates with Zr and/or U.

Table 1
Representative metal atoms selected as simulated fission products in UO_2, given in metal at%

Dopant metal	Burnup/at%			
	2 at% [a] (FP2A)	5 at% [a] (FP5A)	10 at% [b] (FP10A)	10 at% [c] (FP10B)
U	98.21	95.52	91.01	89.67
Zr	0.74	1.86	3.73	2.33
Ce	0.25	0.62	1.24	3.69
Pr	0.12	0.30	0.61	0.50
Nd	0.58	1.46	2.93	3.05
Y	0.10	0.24	0.49	0.26
Sr	–	–	–	0.50

[a] Concentrations based on the yield of stable or long-lived fission products, which are thought to be soluble in UO_2 [11]. [b] Previous sample reported in Ref. 6. [c] Concentrations calculated from the ORIGEN-II computer code.

Therefore in the case of the B series of the FP10B (10 at% burnup) sample, the six elements including Sr, in addition to the five elements in the A series, were selected for the simulation of the fission products equivalent to 10% burnup, the concentrations of which were determined from the ORIGEN-II computer code calculation.

The samples of the A series were prepared as follows. The metal oxide powder simulating the fission products and UO_2 powder were mixed mechanically and then shaped into a cylindrical rod about 7 mm in diameter and 50 mm in length using an evacuated rubber press with a hydrostatic pressure of about 400 MPa. The cylindrical rod was sintered and homogenized at 1623 K for 7 days in an Ar gas flow and then at 1273 K for 1 day in a dry hydrogen gas flow so as to obtain the stoichiometric composition (the ratio of oxygen to metal, $O/M = 2.00 \pm 0.01$) according to the previous thermogravimetric study on the relation between the O/M ratio and the oxygen partial pressure [12]. This sintering and homogenizing process was repeated several times. The densities of the samples, measured by immersion, were 86.7% (FP2A) and 97.4% (FP5A) of the theoretical density.

Samples of the B series were made as follows. The mechanically mixed oxide powder was pressed into a cylindrical rod about 10 mm in diameter and 60 mm in length using a large, long die, and sintered at 2053 K for 7 h in a wet hydrogen flow to attain the stoichiometric composition. The density of the sample (FP10B) was 96.7% of the theoretical density.

For each sample rod in both the A and B series, X-ray diffraction analysis showed the presence of a single fluorite phase. The homogeneity of the doped samples was investigated from the split of the α_1 and α_2 peaks at around $2\theta = 125$–128° in the X-ray diffraction pattern, as usual. The X-ray diffraction patterns of doped UO_2 samples (FP2A, 5A, 10A, 10B) are shown in Fig. 1 in comparison with that of undoped UO_2. It is seen in the figure that the split of the α_1 and α_2 peaks gradually becomes unclear with increasing dopant content in the A series. However, the split of the FP10B sample is very clear and much the same as that of undoped UO_2 made by the same preparation method. Typical scanning electron micrographs of the etched samples FP5A and FP10B are shown in Fig. 2. Although the average grain size (20–27 μm) of the FP10B sample is seen to be larger than that (9–10 μm) of the FP5A sample due to the difference in sintering temperature, there seems to be no second phase (or precipitates) and no crack along the grain boundary in the sample rod. It is noted that the black points on the matrix grains are not the precipitates but concavities formed during polishing the sample surface, because the micrograph of pure UO_2 also shows the black points. It is, therefore, concluded that the distribution of dopants in the FP10B sample is quite homogeneous and better than in the FP10A sample and the other A series samples. The A series samples, nevertheless, are thought to be still useful for the heat capacity measurements and the effect of the difference in the homogeneity of the sample shown in Figs. 1 and 2 on the heat capacity may be small, because heat capacity is a bulk property rather than a transport property such as the diffusion coefficient and thermal diffusivity. The negligibly small effect of the difference in two samples (FP10A and FP10B) on the heat capacity is shown in the next section.

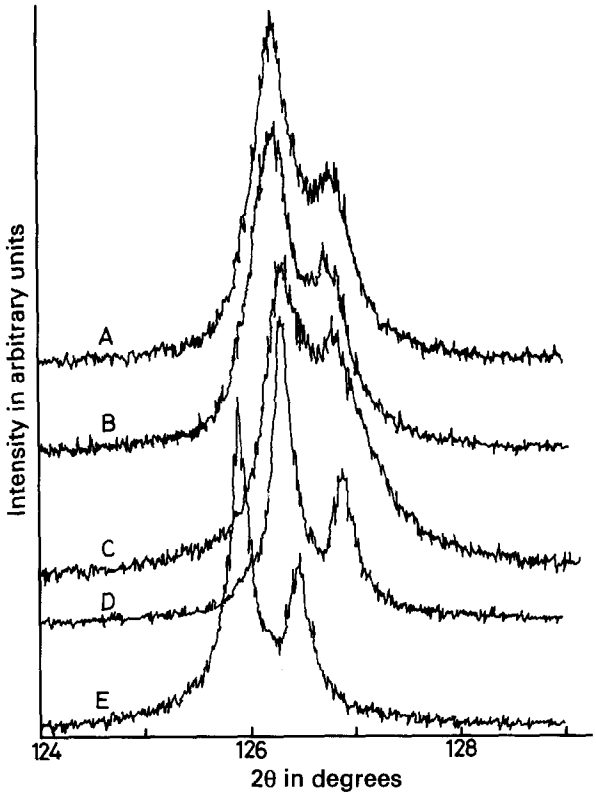

Fig. 1. X-ray diffraction patterns of two series of samples (FP2A, 5A, and 10A, and 10B) and pure UO_2: curve A, FP2A; curve B, FP5A; curve C, FP10A; curve D, FP10B; curve E, pure UO_2.

3. Results and discussion

The heat capacities of UO_2 doped with simulated fission products equivalent to 2 and 5 at% (FP2A and FP5A) and undoped UO_2 measured in this study are shown in Fig. 3 together with that of 10 at% burnup (FP10A) previously reported by the present authors [6]. Although no anomaly is seen in the heat capacity curve of undoped UO_2, an anomalous increase in the heat capacity curve of each sample of $(U_{1-y}FP_y)O_2$ ($y = 0.018$ for 2 at% burnup and $y = 0.045$ for 5 at% burnup) is seen above 1300 and 900 K, respectively, similarly to the previous result of $(U_{0.910}FP_{0.090})O_2$ for 10 at% burnup (FP10A) [6]. The onset temperatures of the heat capacity anomalies decrease with increasing amount of simulated fission products in UO_2. The heat capacity of the 10% burnup sample (FP10B) measured in this study is shown in Fig. 4 in comparison with those of FP10A, undoped UO_2 and $(U_{1-y}M_y)O_2$ (M is Gd [2], La [3], Eu [5]). It is seen in the figure that the presence of an anomalous increase in the heat capacity curve, the onset temperature of an anomalous increase and the temperature dependence of the heat capacity of

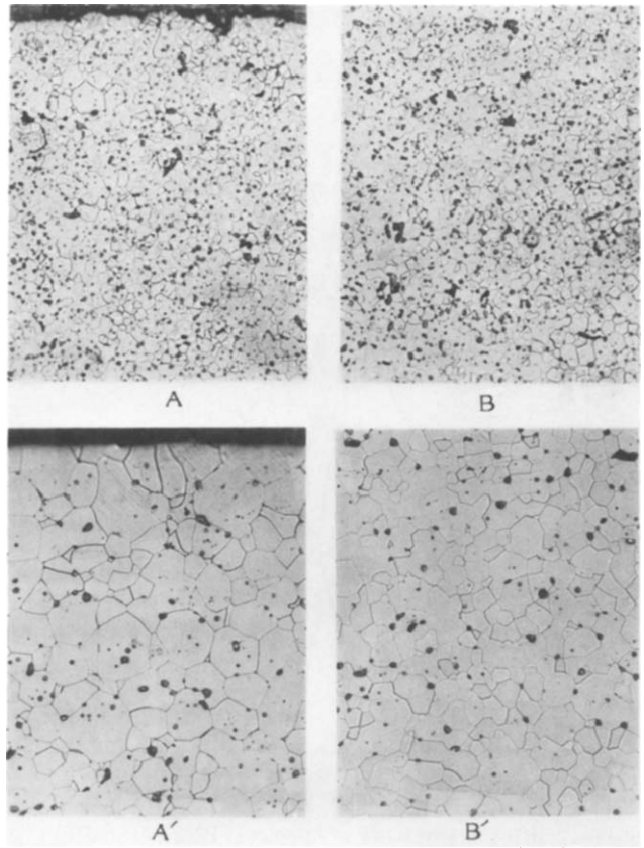

Fig. 2. Scanning electron micrographs of the samples FP5A (A, B) and FP10B (A′, B′) after etching (original magnification × 400): A and A′, peripheral parts of a sample rod; B and B′, central parts.

FP10B are in excellent agreement with those of FP10A, regardless of the difference in sample preparation methods and dopant elements (with or without inclusion of Sr), although the difference in dopant composition is small as seen in Table 1. The anomalous increase in the heat capacity curve is, therefore, not considered to be a sample-dependent phenomenon, i.e. not due to inhomogeneity in the distribution of the dopants, but is inherent in the presence of dopants in the sample. It is also seen that the onset temperatures (T_r) of the heat capacity anomaly of $(U_{1-y}FP_y)O_2$ are far lower than those of UO_2 doped with a single kind of cation with the same dopant content.

The excess heat capacity was evaluated by subtracting the smoothed base line of heat capacity from the experimental values above the onset temperature. The smoothed base line was determined by applying a least-squares fitting for the data in the temperature range below the onset temperature and then extrapolating a fitted line to the range above the onset temperature. Assuming that the excess heat capacity is due to the formation of Frenkel pairs of oxygen, similarly to the cases

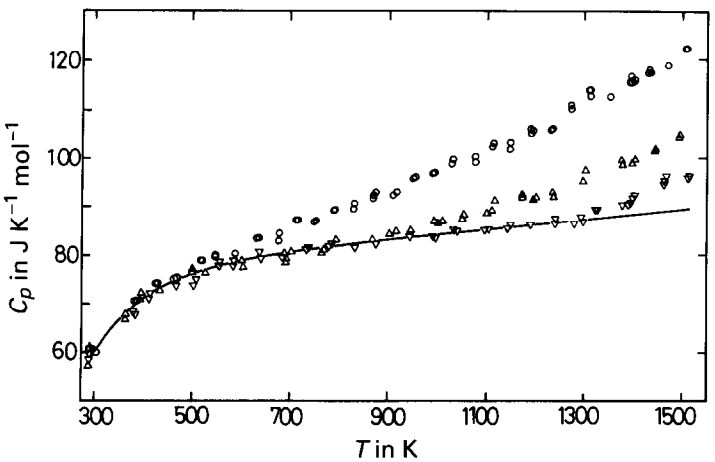

Fig. 3. Temperature dependences of the heat capacities of the simulated fission products equivalent to 2, 5, 10 at% burnup: ▽, FP2A (this study); △, FP5A (this study); ○, FP10A [6]; ——, undoped UO_2 (this study and Refs. [6] and [10]).

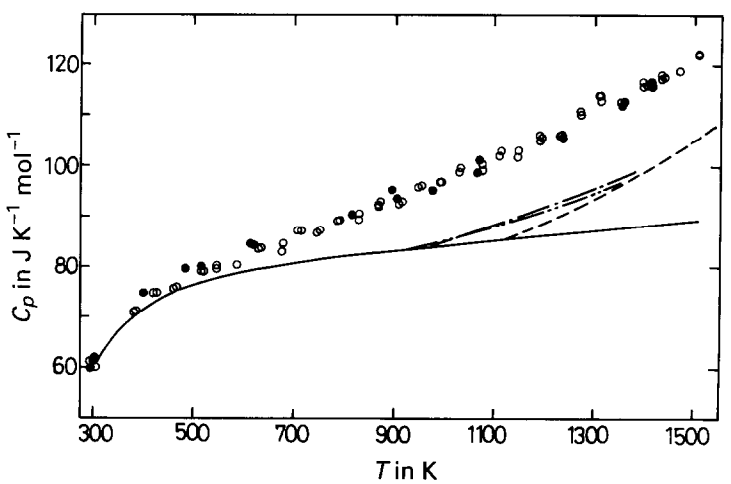

Fig. 4. Temperature dependences of the heat capacities of $(U_{0.910}FP_{0.090})O_2$ and $(U_{0.910}M_{0.090})O_2$: ○, FP10A [6]; ●, FP10B (this study); — · · —, $U_{0.899}Gd_{0.101}O_2$ [2]; – – –, $U_{0.910}La_{0.090}O_2$ [3]: — · —, $U_{0.910}Eu_{0.090}O_2$ [5]; and ——, undoped UO_2 (this study and Refs. [6] and [10]).

of Gd-, La-, Sc-, Eu- and Y-doped UO_2 [2–6], the excess heat capacity ΔC can be expressed as [13]

$$\Delta C = [(\Delta H_f)^2/(\sqrt{2}RT^2)] \exp(\Delta S_f/2R - \Delta H_f/2RT) \quad (1)$$

where ΔS_f and ΔH_f are the entropy and enthalpy of Frenkel-pair formation, respectively. The enthalpy and entropy of Frenkel-pair formation in $(U_{1-y}FP_y)O_2$ obtained from Eq. (1) in this study and in Ref. 6 are shown in Figs. 5 and 6,

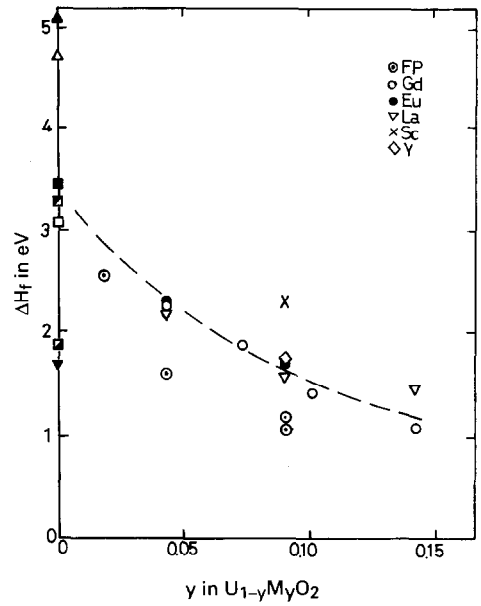

Fig. 5. Enthalpy of defect formation: ⊙, $(U_{1-y}FP_y)O_2$ (this study and Ref. [6]); ○, $(U_{1-y}Gd_y)O_2$ [2]; ▽, $(U_{1-y}La_y)O_2$ [3]; ×, $(U_{0.910}Sc_{0.090})O_2$ [4]; ●, $(U_{1-y}Eu_y)O_2$ [5]; ◇, $(U_{0.910}Y_{0.090})O_2$ [6]; ▲, theoretical value for the formation of a Frenkel pair [15]; △, from a neutron-scattering study [16]; □, Ref. [13]; ◩, Ref. [14]; and ■, Ref. [17], three values from the excess heat capacity of UO_2; ◪, calculated value for the formation of an electron-hole pair [18]; ▼, theoretical value for the formation of an electron-hole pair [15].

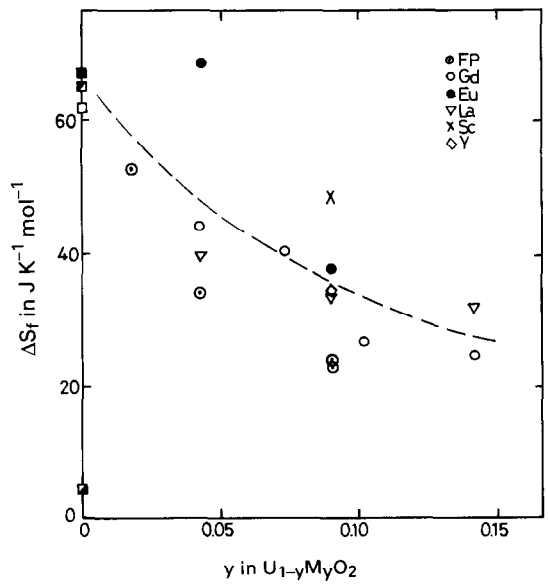

respectively, together with those of UO_2 [13–19] and $(U_{1-y}M_y)O_2$ (M is Gd, La, Sc, Eu, Y) reported previously [2–6]. The values of enthalpy and entropy in both samples FP10A and 10B are seen to be in good agreement (FP10A: $\Delta H_f = 1.1 \pm 0.1$ eV, $\Delta S_f = 23 \pm 1$ J mol^{-1} K^{-1}; and FP10B: $\Delta H_f = 1.2 \pm 0.1$ eV, $\Delta S_f = 24 \pm 1$ J mol^{-1} K^{-1}) as expected from almost the same temperature dependence of the heat capacity in Fig. 4. But the values are seen to be a little lower than those of UO_2 doped with a single cation (M), i.e. $(U_{1-y}M_y)O_2$, suggesting the possibility of a somewhat different mechanism for the heat capacity anomaly from that of $(U_{1-y}M_y)O_2$. However, as seen in these figures, the extrapolation of both values for $(U_{1-y}FP_y)O_2$ and $(U_{1-y}M_y)O_2$ to zero dopant content ($y = 0$) yields almost the same values as for undoped UO_2 ($\Delta H_f \approx 3$ eV and $\Delta S_f \approx 60$ J mol^{-1} K^{-1}) which are in good agreement with the experimental values of undoped UO_2 reported so far [13,14,17], implying that the principal mechanism for the heat capacity anomaly among undoped UO_2, $(U_{1-y}M_y)O_2$ and $(U_{1-y}FP_y)O_2$ is not significantly different. The values of ΔH_f for undoped UO_2 in Fig. 5 thus obtained by extrapolation are higher than the enthalpy of formation of an electron-hole pair calculated theoretically by Harding et al. [15], but lower than that of a Frenkel pair of oxygen also calculated theoretically by Harding et al. [15]. In Fig. 6, the extrapolated value of ΔS_f for undoped UO_2 obtained in this study is seen to be higher than the entropy of formation of an electron-hole pair estimated by Hyland and Ralph [18]. It is noted that the values of enthalpy and entropy of defect formation calculated from the same excess heat capacity estimated in this study, assuming the presence of an electron-hole pair formation, are equal to and 5.8 J K^{-1} mol^{-1} larger than those respective values for a Frenkel-pair formation mentioned above. Therefore, regardless of the defect model, the same conclusion that the entropy value is different from that for an election-hole pair formation can be obtained.

The electrical conductivities of $(U_{1-y}FP_y)O_2$ were measured simultaneously with a direct heating pulse calorimeter in order to detect the occurrence of electron-hole pair formation around the onset temperatures of the heat capacity anomaly and the results are shown in Fig. 7, where the onset temperatures of the anomalous increase in the heat capacity are shown by the vertical arrows. In the electrical conductivity curves of all the samples of $(U_{1-y}FP_y)O_2$ ($y = 0.018$, 0.045 and 0.090 (FP10A and 10B)), it is clear that there is no slope change at the temperature where the heat capacity increases anomalously. It is, therefore, not likely that the excess heat capacity of $(U_{1-y}FP_y)O_2$ is due to the formation of electron-hole pairs. The higher electrical conductivity of FP10B than that of FP10A may be due to the better homogeneity of the dopant in the UO_2 matrix, as seen in the X-ray diffraction patterns in Fig. 1.

Fig. 6. Entropy of defect formation: ○, $(U_{1-y}FP_y)O_2$ (this study and Ref. [6]); ○, $(U_{1-y}Gd_y)O_2$ [2]; ▽, $(U_{1-y}La_y)O_2$ [3]; ×, $(U_{0.910}Sc_{0.090})O_2$ [4]; ●, $(U_{1-y}Eu_y)O_2$ [5]; ◇, $(U_{0.910}Y_{0.090})O_2$ [6]; □, Ref. [13]; ◩, Ref. [14]; and ■, Ref. [17], three values from the excess heat capacity of UO_2; ◪, calculated value for the formation of an electron-hole pair [18].

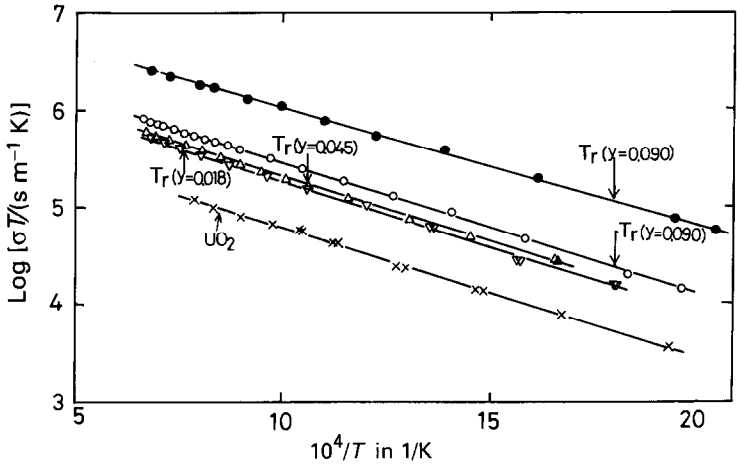

Fig. 7. Electrical conductivity of UO_2 and $(U_{1-y}FP_y)O_2$: × – ×, undoped UO_2; ▽ – ▽, $y = 0.018$ (FP2A); △ – △, $y = 0.045$ (FP5A); ○ – ○, $y = 0.090$ (FP10A); ● – ●, $y = 0.090$ (FP10B).

In Fig. 8, the onset temperatures (T_r) of the heat capacity anomaly of $(U_{1-y}FP_y)O_2$ are plotted against $|\Delta a|$ together with those of UO_2 doped with various cations [2–6], where $|\Delta a|$ is the lattice parameter change per mol% of

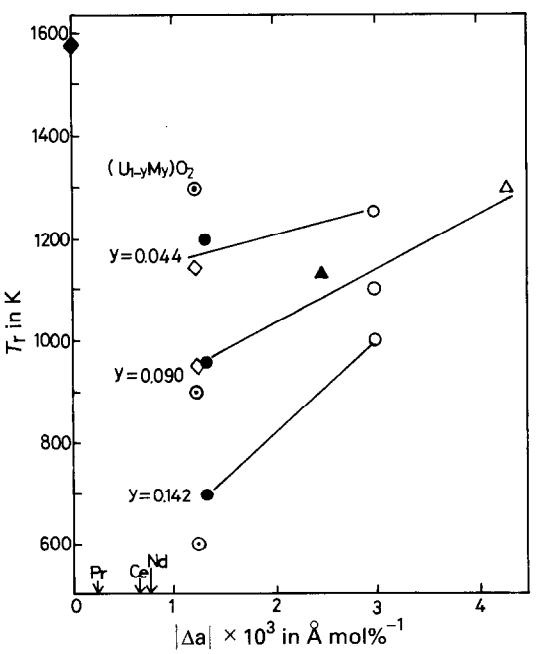

Fig. 8. Relation between the onset temperature of the heat capacity anomaly and the change in the lattice parameter of doped UO_2 per mol% of dopant: ⊙, $(U_{1-y}FP_y)$ (this study and Ref. [6]); ●, Gd [2]; ○, La [3]; △, Sc [4]; ◇, Eu [5]; ▲, Y [6]; ◆, undoped UO_2 estimated in Ref. [19].

dopant in doped UO_2 calculated from the experimental values reported previously [12,20–24]. It is seen in this figure that the onset temperature of doped UO_2 with constant dopant concentration (y), except for $(U_{1-y}FP_y)O_2$, increases linearly with increasing $|\Delta a|$, indicating that the smaller elastic strain decreases the onset temperature of the heat capacity anomaly. The fact that the ionic conductivity of doped fluorite-type oxides, such as ZrO_2 doped with trivalent cations where the oxygen ion is the predominant mobile species, decreases with increasing $|\Delta a|$ as reviewed by Kim [25], also supports the dependence of the onset temperature upon the $|\Delta a|$ value, because the Frenkel-pair-like defect of oxygen can be formed more easily under the condition that makes oxygen ions more mobile. The onset temperatures of $(U_{1-y}FP_y)O_2$, however, are seen to be apart from the straight line drawn by using the onset temperatures of UO_2 doped with a single cation. Although the lower onset temperatures of $(U_{1-y}FP_y)O_2$ are not easy to explain at present, they may be related to the combined effect of the small $|\Delta a|$ of UO_2 doped with trivalent Ce, Pr and Nd [26–28], as shown in the abscissa in Fig. 8, and/or tetravalent Ce and Zr, and/or caused by the variety of the local structures composed of the dopant ions, uranium ions and oxygen ions in UO_2, i.e. the variety of U–M, M–M, M–O, U–O and O–O interatomic distances, coordination numbers and bonding strength. Heat capacity measurements of UO_2 doped with one kind of these special dopants (Ce, Pr, Nd or Zr) and precise X-ray analyses of the crystal structures are now in progress in our laboratory.

It is concluded that the anomalous increase in the heat capacity of $(U_{1-y}FP_y)O_2$ is inherent and does not depend on the sample character. The onset temperature of the heat capacity anomaly observed for $(U_{1-y}FP_y)O_2$ increases with increasing dopant concentration (y value). The anomalous increase in the heat capacity is thought to originate from a mechanism similar to that observed for $(U_{1-y}M_y)O_2$ (M is a single cation such as Gd, La, Eu, Sc and Y). The predominant thermally activated process in the origin of the excess heat capacity is likely to be the formation of the Frenkel-pair-like defect of oxygen. The fact that the onset temperatures of $(U_{1-y}FP_y)O_2$ are lower than those of $(U_{1-y}M_y)O_2$ is probably related to the variety of the local structures of the dopant in UO_2.

Acknowledgements

The authors are indebted to Nippon Nuclear Fuel Development Co., Ltd. for the supply of UO_2 samples (FP10B) and the sample analysis by X-ray and scanning electron micrograph.

References

[1] J.C. Killeen, J. Nucl. Mater., 58 (1975) 39.
[2] H. Inaba, K. Naito and M. Oguma, J. Nucl. Mater., 149 (1987) 341.
[3] T. Matsui, Y. Arita and K. Naito, J. Radioanal. Nucl. Chem., 143 (1991) 149.
[4] T. Matsui, Y. Arita and K. Naito, Solid State Ionics, 49 (1991) 195.

[5] T. Matsui, T. Kawase and K. Naito, J. Nucl. Mater., 186 (1992) 254.
[6] T. Matsui, Y. Arita and K. Naito, J. Nucl. Nucl. Mater., 188 (1992) 205.
[7] K.C. Mills, F.H. Ponsford, M.J. Richardson, N. Zaghini and P. Fassina, Thermochim. Acta, 139 (1989) 107.
[8] P.G. Lucuta, H.J. Matzke, R.A. Verrall and H.A. Tasman, J. Nucl. Mater., 188 (1992) 198.
[9] K. Naito, H. Inaba, M. Ishida and K. Seta, J. Phys. E, 12 (1979) 712.
[10] F. Grønvold, N.J. Kveseth, A. Sveen and J. Tichy, J. Chem. Thermodyn., 2 (1970) 655.
[11] M.E. Meek and B.F. Rider, Technical Report NEDO-12154, General Electric Company, CA, 1972.
[12] K. Une and M. Oguma, J. Nucl. Sci. Technol., 20 (1983) 844.
[13] R. Szwarc, J. Phys. Chem. Solids, 30 (1969) 705.
[14] J.P. Kerrisk and D.G. Clifton, Nucl. Technol., 16 (1972) 531.
[15] J.H. Harding, P. Masri and A.M. Stoneham, J. Nucl. Mater., 92 (1980) 73.
[16] K. Clausen, W. Hayes, J.E. MacDonald and R. Osborm, Phys. Rev. Lett., 52 (1984) 1238.
[17] P. Browning, J. Nucl. Mater., 98 (1981) 345.
[18] G. Hyland and J. Ralph, High Temp.-High Press., 15 (1983) 179.
[19] T. Matsui and K. Naito, J. Nucl. Mater. 138 (1986) 19.
[20] C. Miyake, H. Amada and S. Imoto, J. Nucl. Sci. Technol., 23 (1986) 326.
[21] W.B. Wilson, C.A. Alexander and A.F. Gerds, J. Inorg. Nucl. Chem., 20 (1961) 242.
[22] Y. Hinatsu and T. Fujino, J. Solid State Chem., 62 (1986) 342.
[23] C. Miyake, T. Isobe and S. Imoto, J. Nucl. Mater., 152 (1988) 64.
[24] L.N. Grossman, J.E. Lewis and D.M. Rooney, J. Nucl. Mater., 21 (1976) 302.
[25] D.J. Kim, J. Am. Ceram. Soc., 72 (1989) 1415.
[26] T. Ohmichi, S. Fukushima, A. Maeda and H. Watanabe, J. Nucl. Mater., 102 (1981) 40.
[27] T. Fujino, J. Nucl. Mater., 154 (1988) 14.
[28] T. Yamashita, T. Fujino and H. Tagawa, J. Nucl. Mater., 132 (1985) 192.